JOURNAL OF PROPULSION AND POWER
Vol. 25, No. 3, May–June 2009

Experimental Investigation of a Novel Combustor Model for Gas Turbines

M. J. Melo,* J. M. M. Sousa,† and M. Costa‡
Technical University of Lisbon, 1049-001 Lisbon, Portugal
and
Y. Levy§
Technion—Israel Institute of Technology, 32000 Haifa, Israel

DOI: 10.2514/1.35173

The present study describes the performance of a novel combustor model for gas turbines. The working principle of this combustor is based on the establishment of a large recirculation zone in the combustion chamber, where part of the inlet air is mixed with the combustion products. Efficient mixing is achieved by the use of high-velocity inlet air jets. Six different inlet air geometries have been analyzed under nonreacting and reacting conditions at atmospheric pressure. Laser-Doppler anemometry was employed to characterize the mean velocity and turbulent kinetic energy fields as a function of the air mass flow rate and geometry configuration. Measurements of mean gas species concentration (O_2, CO_2, CO, HC, and NO_x) at the model exhaust are reported as a function of the equivalence ratio for all configurations. The isothermal data revealed that the recirculation ratio is mainly a function of the geometry, with a minor dependence on the experimental conditions. Under reacting conditions, the data revealed that NO_x emissions are low regardless of the combustor operating conditions and geometry. However, the air inlet configuration has a strong effect in combustor efficiency.

Nomenclature

A_R	=	area section, m^2
A_{R1}	=	area section, m^2
k	=	turbulent kinetic energy, m^2/s^2
$\dot{m}_f$	=	fuel mass flow rate, kg/s
$\mathbf{N}$	=	unit normal vector
Q_{air}	=	airflow rate, m^3/s
R	=	recirculation ratio
$\overline{u^2}$, $\overline{v^2}$	=	velocity variances, m^2/s^2
$\mathbf{V}$	=	mean velocity vector, m/s
x, y	=	spatial coordinates, m
ρ_{air}	=	air density, kg/m^3
ϕ	=	equivalence ratio

I. Introduction

GAS turbines are the preferred choice for aeroengines because of the tremendous advantages offered, namely in terms of range, speed, and reliability. Furthermore, the use of gas turbines in propulsion systems for other applications is still growing, especially in shipping transportation. To a great extent, this is a result of the steady increase in the efficiency of gas turbines, despite increasingly more demanding emissions regulations. In fact, the hot primary zone within the combustor and the high turbine inlet temperatures, a crucial factor for increased efficiency, promote the formation of nitrogen oxides (NO_x). To overcome this problem, a variety of methods have been used [1–5]. Some of these were directly related to the combustion chamber, such as fuel or air staging, catalytic combustion, lean-premixed prevaporized (LPP) combustion, and rich burn-quick quench-lean burn (RQL) combustion. Other methods were applied to postcombustion flue gas, such as selective catalytic reduction and selective noncatalytic reduction. The fuel or air staging technology introduces additional mechanical complexity and control problems, and the reduction of pollutant emissions is only moderate. Catalytic combustion can reduce NO_x emissions by several orders of magnitude, as demonstrated in subscale rigs for typical gas turbine operating conditions. However, this technology is not easily applicable to nonstationary gas turbines, particularly in the operation of aircraft engines at high inlet temperatures and high fuel–air ratios. Additional drawbacks may also be noted, such as the development of thermal instabilities and reduced durability and fuel flexibility. The LPP combustion presents safety problems associated to the risk of damage by flashback or autoignition of the air–fuel mixture, particularly when using liquid fuels. Moreover, LPP combustors should not be used at high air inlet temperatures (higher risk of flashback or autoignition) and are prone to combustion instabilities that may reduce their lifetime. In the context of the lean-premixed combustion, the work of Hsu et al. [6] and Roquemore et al. [7] on the trapped vortex combustor must be mentioned. Using such approach, these authors have obtained emissions of 10 ppm NO_x and 10 ppm CO (both corrected for 15% O_2 concentration) along with high combustion efficiencies (>99.9%). The RQL combustion has been successful in the reduction of NO_x emissions from fuel-bound nitrogen and in avoiding thermal NO formation. However, this technology requires physical separation of the combustor into two chambers and an intermediate passage referred to as a quenching zone. A large amount of soot is generated in the primary zone, causing high radiative fluxes to the walls and cooling problems. It is also difficult to ensure an effective and uniform quenching between the rich and the lean zones. As a consequence of all these difficulties, it may be concluded that there is still a great need for low-cost, safe, and reliable NO_x reduction methods, especially for high-efficiency, small gas turbine engines.

This study deals with an innovative combustion chamber that is aimed at achieving the ultralow NO_x class (less than 10 ppm) with improved efficiency. It is based on the establishment of a large internal recirculating combustion zone where the fuel is injected. The amount of burnt recirculated gases is limited to a certain value, above which the flame becomes unstable and eventually extinguishes [8]. However, if the temperature of the mixture of the recycled exhaust

Received 16 October 2007; revision received 6 October 2008; accepted for publication 6 October 2008.

*Postdoctoral Scholar, Instituto Superior Técnico, Mechanical Engineering Department, Avenida Rovisco Pais.
†Assistant Professor, Instituto Superior Técnico, Mechanical Engineering Department, Avenida Rovisco Pais. Senior Member AIAA.
‡Associate Professor, Instituto Superior Técnico, Mechanical Engineering Department, Avenida Rovisco Pais.
§Professor, Faculty of Aerospace Engineering.

gas and fresh air exceeds that of the fuel autoignition, the limits for stable combustion extend to much higher recirculation ratios and continuous combustion is sustained [9]. Based on previous experimental work [10–15], it was concluded that the key issue in this method is the dilution of combustion air with combustion products before mixing between fuel and combustion air. Combustion takes place in an atmosphere of low oxygen concentration because of the previous dilution of air with combustion products. This may be accomplished, as in the present work, by promoting the recirculation of combustion products via high-velocity inlet air jets. In contrast to classic diffusion flames, temperature peaks can thus be avoided, even at high preheated air temperatures, a necessary condition to obtain significant efficiency gains. This combustion mode is characterized by a moderate and distributed temperature rise, small gradients of temperature and species, low pollutant emissions and noise, and relatively uniform radiative fluxes. The improved aerodynamics of the internal combustor also has the potential to produce more uniform wall temperatures, leading to less stringent wall-cooling requirements and lower thermal stresses.

This article examines the performance of a novel combustor model for gas turbines. Six different inlet air geometries have been analyzed under nonreacting and reacting conditions at atmospheric pressure. Laser-Doppler anemometry was employed to characterize the mean velocity and turbulent kinetic energy fields as a function of the air mass flow rate and geometry configuration. Measurements of major gas species concentrations at the model exhaust are reported as a function of the equivalence ratio for all configurations.

II. Experimental Apparatus and Procedure

Figure 1 shows the three different combustion chamber configurations used in the development and optimization of the present combustor. They are as follows:

Fig. 1a shows the original configuration, with a single variant (model O).

Fig. 1b presents configuration A, with three variants (models A1, A2, and A2SH).

Fig. 1c shows configuration B, with two variants (models B1 and B2).

As illustrated in Fig. 1, the differences among the three configurations lie in the geometry of the air inlet for the experimentally investigated 60-deg sectors of the combustion chamber. In each configuration, the models differ in the specific shape of the inlet air section. Figure 2 shows the cross section of the combustion chamber of model O; the schematics for the other models are similar, with the exception of the air inlets geometry (as described later in this section). A common feature to all configurations is the geometry of the fuel injection and the exhaust section. The injection system is formed by 15 1-mm circular holes with a spacing of 2 mm. The fuel (methane) was injected through these holes into the combustion chamber at an angle of 45 deg with respect to the y axis, as schematically depicted in Fig. 2. Key dimensions shared by all configurations are also shown in this figure. In model O, the air is admitted into the combustion chamber through two slots (Figs. 1a). The right slot is parallel to the exhaust channel and the left one is perpendicular to it, being that the inlet areas of both slots are the same. In configuration A, the air enters the combustion chamber through 14 6-mm circular holes (Figs. 1b). The air inlets make angles of 120 and 210 deg with respect to the y axis in the right and left sections, respectively. In model A1, the holes in the right section are aligned with those in the left section, whereas model A2 displays a staggered arrangement. Model A2SH differs from model A2 in the diameter of the holes only, which have been reduced to 4 mm. Configuration B shows the same left inlet section as configuration A, but the holes in the right section are parallel to the exhaust channel and exhibit a semicircular geometry instead (Figs. 1c). Similar to variants A1 and A2, models B1 and B2 correspond to aligned and staggered arrangements of the air inlet holes, respectively.

The isothermal flow in the combustor chamber model was characterized by the application of laser-Doppler anemometry. A two-component velocimeter from Dantec, which was operated in the dual-beam backward-scatter mode, was used to meet this objective [16]. High data rates, close to 1 kHz, were obtained by seeding the flow with 1-μm droplets. These droplets where generated by four medical nebulizers Inspiron 002305, employing an ethyleneglycol (20%) and water (80%) liquid mixture. The transmitting optics had a beam separation of 38 mm and a focal length lens of 400 mm, which generated an ellipsoidal measurement volume containing 35 interference fringes and characterized by major-axis dimensions of 0.19

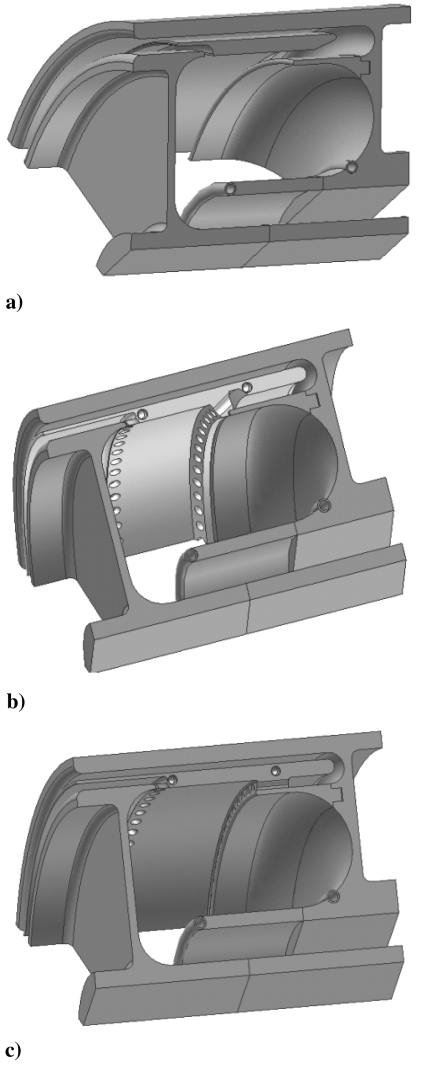

Fig. 1 Combustion chamber configurations: a) original configuration, b) configuration A, and c) configuration B.

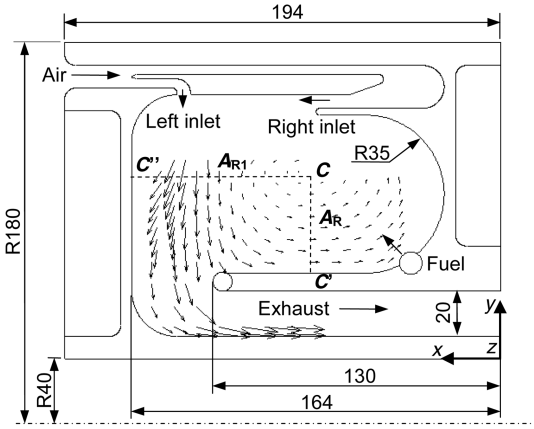

Fig. 2 Cross section schematics and key dimensions of the combustion chamber (model O).

and 3.88 mm, respectively, in the y and z directions (see Fig. 2). The back-scattered light from the droplets was collected by a fiber-optics probe, collecting its light through the same 400-mm focal length lens. Subsequently, the analog signal from the photomultipliers was bandpass filtered and processed by two Dantec 57N20/57N35 Burst Spectrum Analyzers interfaced with a personal computer, using "burst" data collection mode and a record length of 32 samples per burst. Velocity statistics were evaluated by ensemble averaging, calculated from 10,000 samples, using BURSTware software. According to the formulas referred by Yanta and Smith [17], this number of individual velocity measurements led to statistical (random) errors below 1% in mean values, and 2% in standard deviations, for a 95% confidence level interval. Errors incurred in the measurement of velocities by displacement and distortion of the measuring volume due to refraction on the combustor model side walls (20-mm thick optical quartz glass windows) were found to be negligibly small and within the accuracy of the measurement system.

Figure 3 displays the experimental arrangement used for the measurement of the (mean) gas species concentration at the combustor exhaust under reacting conditions. Note that all models were designed to operate within a testing facility (plenum), as shown in Fig. 4, both under nonreacting and reacting conditions. Under reacting conditions, this arrangement allowed the heat losses from the side walls of the combustion chamber to be used to preheat the fresh air.

The species considered in the measurement of the flue-gas data, namely O_2, CO, CO_2, hydrocarbons (HC), and NO_x, were collected using a water-cooled stainless steel probe installed in the exhaust plenum at approximately 1 m downstream from the combustion chamber exit (see Fig. 3), in a location where the gas composition was nearly uniform. The wet sample was drawn through the probe and part of the sampling system by an oil-free diaphragm pump. A condenser removed the main particulate burden and condensate. A filter and a drier removed any residual moisture and particles, so that a constant supply of clean dry combustion gases was delivered to each measurement instrument through a manifold, to obtain species concentrations on a dry basis. The analytical instrumentation included a magnetic pressure analyzer for O_2 measurements, nondispersive infrared gas analyzers for CO_2 and CO measurements, a flame ionization detector for HC measurements, and a chemiluminescent analyzer for the quantification of NO_x. The analog outputs of the analyzers were transmitted via analog/digital (A/D) boards to a computer where the signals were processed and the mean

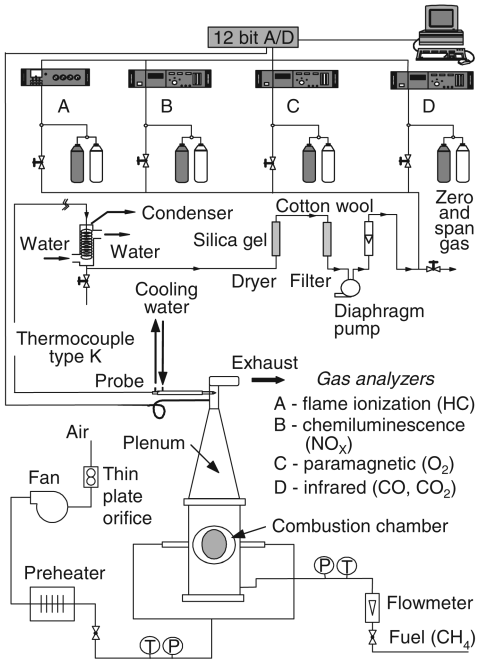

Fig. 3 Experimental apparatus for combustion measurements.

Fig. 4 Photographs of the experimental facility: a) combustion chamber model, b) the assembled combustion chamber model mounted on the interface section to the testing facility, and c) testing facility assembled and incorporating the combustion chamber model.

values calculated. Zero and span calibrations with standard mixtures were performed before and after each measurement session. The maximum drift in the calibration was within ±2% of the full scale. At the combustor exit, where the gas composition was nearly uniform, probe effects were negligible and errors arose mainly from quenching of chemical reactions and sample handling. Samples were quenched near the probe tip to about 150°C, and condensation of water within the probe was avoided by controlling the inlet temperature of the cooling water (typically to around 60°C). Repeatability of the flue-gas data, which constitutes a good indicator of measurement uncertainty, was, on average, within 5%.

III. Results and Discussion

The working principle of the present combustor is based on the establishment of a large recirculation zone in the combustion chamber, where part of the inlet air mixes with the combustion products, as depicted in Fig. 5. The fresh air is split at junction 1 and part of it is stirred with the combustion products at junction 2. After the injection of fuel in the diluted air mixture at junction 3, and if its temperature exceeds the fuel autoignition temperature, it ignites automatically and continuous combustion is sustained, as suggested by Wünning and Wünning [10]. Subsequently, the combustion products are split at junction 4, partly returning to the recirculation zone via junction 2, and partly mixing with dilution air at junction 5 before exhaust from the combustion chamber, as idealized by Levy et al. [9].

The investigated operating conditions in the experiments under nonreacting and reacting flow are summarized in Tables 1 and 2, respectively. Both experiments were performed at atmospheric pressure.

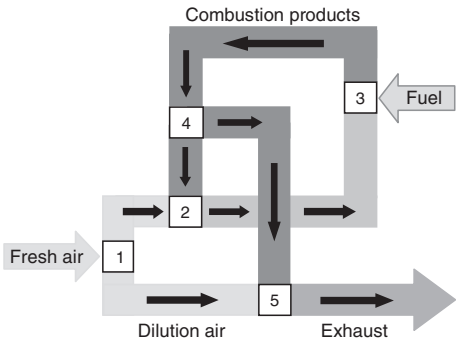

Fig. 5 Working principle of the combustor.

Table 1 Nonreacting operating conditions

Condition	Geometry	Q_{air}, 10^{-2} m^3/s
O1I	O	1.0
O2I		1.7
O3I		2.5
O4I		3.0
A11I	A1	1.0
A12I		1.7
A13I		2.5
A14I		3.0
A21I	A2	1.0
A22I		1.7
A23I		2.5
A24I		3.0
A21SHI	A2SH	1.0
A22SHI		1.7
A23SHI		2.5
A24SHI		3.0
B11I	B1	1.0
B12I		1.7
B13I		2.5
B14I		3.0
B21I	B2	1.0
B22I		1.7
B23I		2.5
B24I		3.0

Table 2 Reacting operating conditions

Geometry	Q_{air}, 10^{-2} m^3/s	$\dot{m}_f$, 10^{-4} kg/s	ϕ
O	1.0–3.0	0.8–4.3	0.07–0.34
A1	1.0–3.0	0.8–4.3	0.07–0.34
A2	1.0–3.0	0.8–3.4	0.07–0.34
A2SH	1.0–2.5	1.2–6.4	0.16–0.47
B1	1.0–3.0	1.2–6.4	0.13–0.35
B2	1.0–3.0	1.2–6.4	0.14–0.47

A. Nonreacting Conditions

The effects of the airflow rate and the different air inlet configurations in the flowfield characteristics have been assessed under nonreacting conditions. Calculated values of the recirculation ratio R were used as a basis for the comparison of the recirculation zones occurring in the various models for different experimental conditions. This parameter is a measure of the fraction of combustion products returning to the recirculation zone, and it was defined as follows:

$$R = \frac{\int_{C-C'} \rho_{air} \mathbf{V} \cdot \mathbf{N}\, dA_R}{\int_{C-C''} \rho_{air} \mathbf{V} \cdot \mathbf{N}\, dA_{R1} - \int_{C-C'} \rho_{air} \mathbf{V} \cdot \mathbf{N}\, dA_R} \tag{1}$$

where ρ_{air} is the density of the air, $\mathbf{V}$ denotes the flowfield velocity vector, and $\mathbf{N}$ stands for the unit vector normal to the integration area. The area sections A_{R1} and A_R are defined in Fig. 2, where point C denotes the center of the recirculation region determined by bivariate (velocity) data interpolation. Another quantity used in the evaluation of isothermal flow conditions was the turbulent kinetic energy k, which is a good indicator of the mixture rates that may be achieved inside the combustion chamber. As only the variances $\overline{u^2}$ and $\overline{v^2}$ corresponding to the velocity components contained in the plane shown in Fig. 2 have been measured, the following approximation has been used:

$$k \approx \tfrac{3}{4}(\bar{u}^2 + \bar{v}^2) \tag{2}$$

The measurements of mean velocity and turbulent kinetic energy at the symmetry plane inside the various models of the combustion chamber, for different operating conditions, are presented in Figs. 6–11. Out-of-plane velocities at this location were negligibly small compared with its reported counterparts, which was verified for a single operating condition by taking oblique measurements using a tilted optical arrangement of the velocimeter. In-plane velocities were quantified at 135 points covering only a limited area as a result of restrictions imposed to optical access by structural restraints. One common characteristic to all investigated flowfields is the existence of a large recirculation zone, with its center located at approximately the same position for each model, irrespective of the variations in airflow rate Q_{air}. In contrast, mean velocities and turbulent kinetic energy always increase with growing values of Q_{air}.

The improvements obtained with model A1 with respect to the original configuration (model O) may be first appreciated by comparing Fig. 7 (experimental conditions A11I, A12I, A13I, and A14I) with Fig. 6 (experimental conditions O1I, O2I, O3I, and O4I). Despite the relatively small change in the mean flow pattern, it can be seen that the characteristic values of turbulent kinetic energy are much higher for the modified configuration. This is a consequence of the smaller area of the air inlets in model A1, thus generating larger local velocity gradients. In addition, the air passage through the circular holes in this configuration leads to the formation of a series of jets from both right and left inlets. These interact with each other, resulting in a significant production of turbulent kinetic energy, which is convected into the recirculation zone. In contradistinction, the performance of model A2 did not present an advance with respect to the previous one. The results for this model are shown in Fig. 8 (experimental conditions A21I, A22I, A23I, and A24I). By staggering the holes of the air inlets in model A2 (see Sec. II), the aforementioned jet interaction seems to have been reduced. As a result, lower levels of turbulence are obtained. However, the mean flow pattern indicates a slightly larger recirculation zone, which may have a small positive impact on the calculated value of R. The

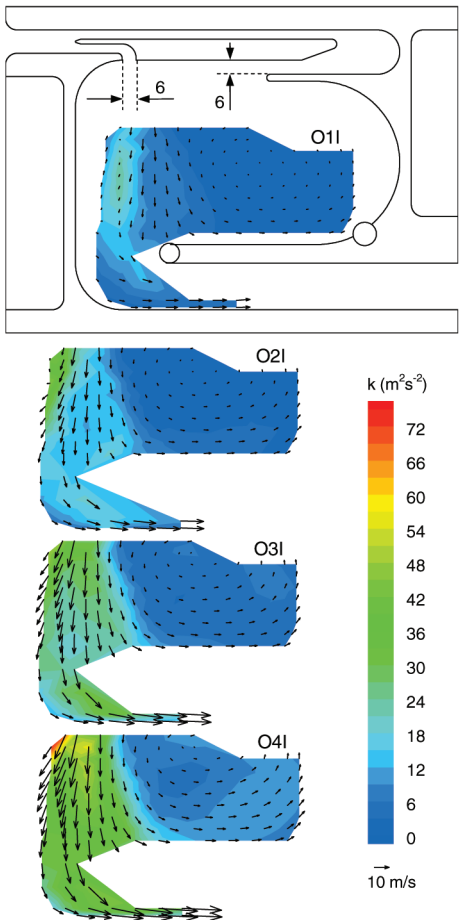

Fig. 6 Mean velocity vectors and turbulent kinetic energy fields at the symmetry plane inside the combustion chamber for the original configuration (model O).

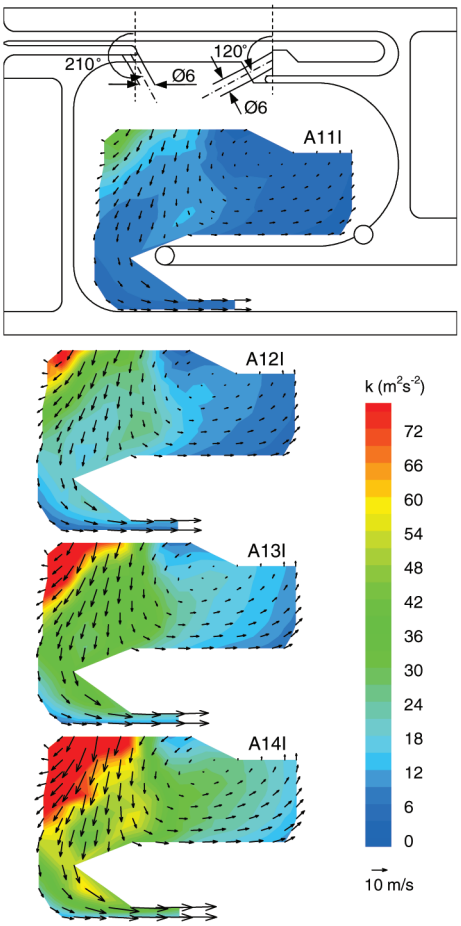

Fig. 7 Mean velocity vectors and turbulent kinetic energy fields at the symmetry plane inside the combustion chamber for model A1.

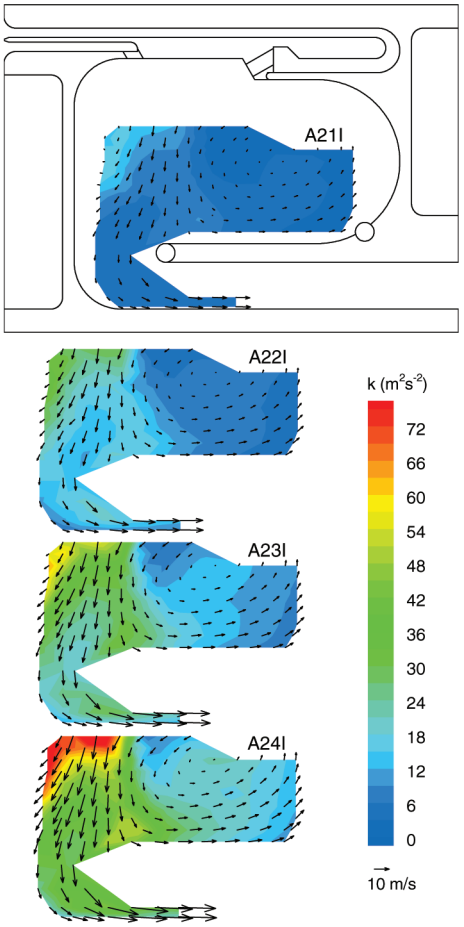

Fig. 8 Mean velocity vectors and turbulent kinetic energy fields at the symmetry plane inside the combustion chamber for model A2.

two-thirds reduction in hole size operated in model A2SH with respect to the previous variant (see Sec. II) was an attempt to counteract the aforementioned decrease of the turbulent kinetic energy. The results for this model are shown in Fig. 9 (experimental conditions A21SHI, A22SHI, A23SHI, and A24SHI). In fact, an improvement is obtained, though the turbulence levels inside the recirculation zone are still lower than those observed in model A1. Furthermore, an increase of the local mean velocities can also be noted in that area, which may be translated into additional gains in R.

The use of configuration B has allowed a major increase in the dimensions of the recirculation zone, as a direct consequence of the change in orientation of the right air inlet (see again Sec. II). The results for model B1 are shown in Fig. 10 (experimental conditions B11I, B12I, B13I, and B14I). It can be concluded that the aforementioned alteration in the mean flow pattern has been obtained at the expense of the levels of turbulent kinetic energy, which are considerably lower for this model. The transport of k into the recirculation zone is much reduced in configuration B and, although model B2 provided an improvement with respect to B1 at low values of Q_{air}, further reductions occur at higher airflow rates. This may be observed in Fig. 11, which displays the results for model B2 (experimental conditions B21I, B22I, B23I, and B24I). Nevertheless, the high values of R that may potentially be obtained with configuration B must be kept in mind.

The calculated values of the recirculation ratio for all the models previously considered are listed in Table 3. It can be concluded from this data that the value of R is mainly a function of the geometry, with a minor dependence on the airflow rate. A significant increase in this parameter with respect to the original model was obtained for configuration A, especially at low Q_{air}. Further improvements for the whole range of studied airflow rates were obtained with model A2 and, particularly, model A2SH. However, as expected from the previous analysis of the mean flow patterns, configuration B (both models) exhibits a dramatic increase in R, nearly doubling the remaining values. So, on one hand, the large recirculation zone might contribute to improve the performance of the combustor under reacting conditions, lowering the emissions of CO and HC as a result of the higher residence time in the combustion zone. The NO_x emissions should not be affected because the content of O_2 in this area will be low and the temperatures will probably be below 1850 K. On the other hand, due to the low levels of turbulence in configuration B, the transport of fresh air into the recirculation zone will be less effective, thus yielding a reduction in the mixing rates between air, combustion products, and fuel. This is likely to result in improper combustion rates, which, in turn, may lead to the generation of large quantities of unburned HC and CO. Considering the aforementioned, a better performance under reacting conditions is expected from configuration A, particularly for the model A2SH, which combines a high recirculation ratio with improved turbulence levels.

Table 3 Recirculation rates for nonreacting operating conditions

Geometry	R			
	1I	2I	3I	4I
O	0.34	0.45	0.38	0.41
A1	0.56	0.48	0.43	0.46
A2	0.55	0.60	0.53	0.54
A2SH	0.56	0.68	0.61	0.61
B1	1.06	1.08	0.99	0.99
B2	1.12	1.07	0.92	0.92

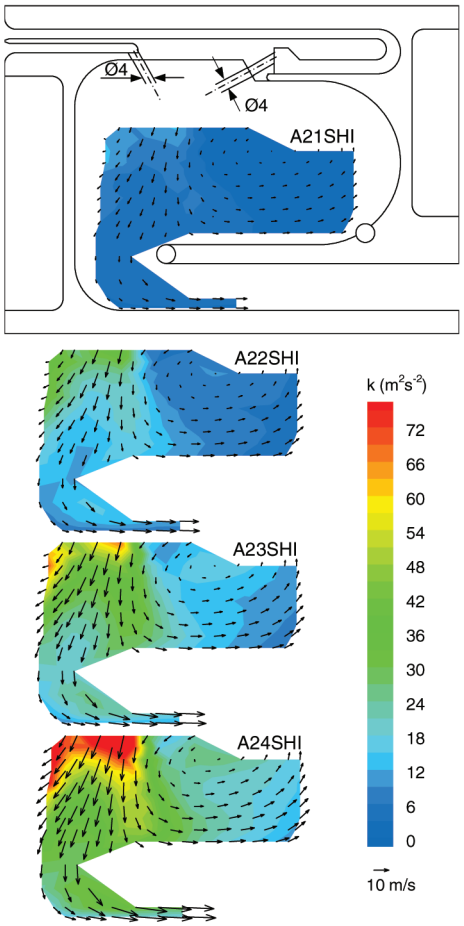

Fig. 9 Mean velocity vectors and turbulent kinetic energy fields at the symmetry plane inside the combustion chamber for model A2SH.

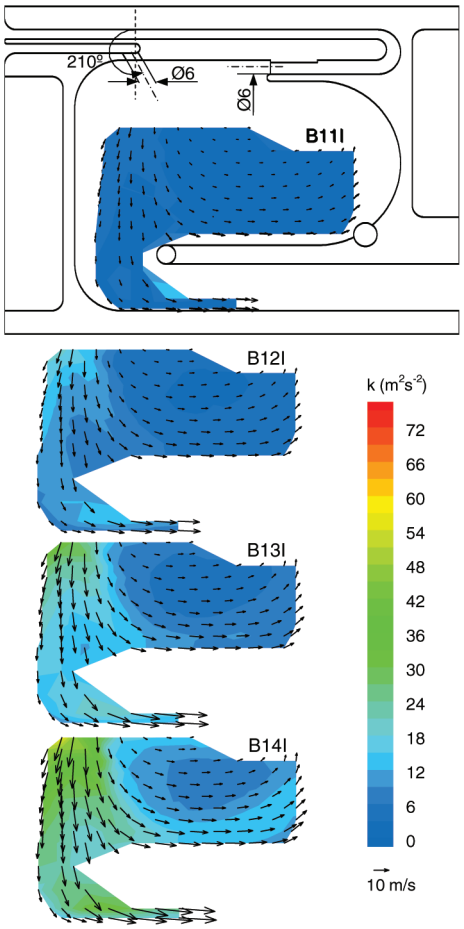

Fig. 10 Mean velocity vectors and turbulent kinetic energy fields at the symmetry plane inside the combustion chamber for model B1.

B. Reacting Conditions

Figures 12–17 show the measurements of the flue gas for all models as a function of the equivalence ratio ϕ. These data demonstrate the great importance of the foregoing parameter in the control of the emissions.

An assessment of the relative performance of the original configuration (model O) and variant A1 can be made by comparing Figs. 12 and 13, respectively, corresponding to the former and latter models. These reveal that CO and HC emissions are significantly lower for model A1. Hence, the combustion efficiency, as defined by Bucher et al. [18], is higher in this case for all experimental conditions. However, higher NO_x emissions are also obtained in model A1. These exhibit values close to 18 ppm at low ϕ, subsequently decaying to approximately 9 ppm for the higher values of ϕ. Corresponding emissions in model O are never above 5 ppm, tending to decrease. This is probably due to a continuous reduction in combustion efficiency at high ϕ. In fact, both models show that CO and HC emissions always increase with ϕ, the increase being particularly pronounced for the latter species. The combustion efficiency is close to 99% for low-power conditions in model A1, but it decreases to merely 80% at high power.

Figure 14 shows the results for model A2, displaying many similarities with those obtained for the first variant of this configuration. Again, CO and, particularly, HC emissions, increase with ϕ. The NO_x emissions in model A2 display values close to 15 ppm at low ϕ, with a further reduction to approximately 6 ppm at high ϕ. These emissions are slightly lower than those observed in the previous model (model A1), which may be a consequence of the moderate increase in the values of R for model A2 (see Table 3). Better results were obtained for model A2SH, as shown in Fig. 15. Contrasting to the previously investigated models, both CO and HC emissions decrease with ϕ in this case, probably due to the higher feeding air injection velocities. In addition, it was possible to achieve higher values of ϕ without the occurrence of combustion in the exhaust channel, thus indicating that more adequate combustion rates result by the use of model A2SH. Higher combustion rates can reduce CO, HC, and NO_x emissions, which usually show an inverse dependency on this quantity. In fact, the emissions of NO_x are generally lower than 10 ppm for this variant and only marginally dependent on ϕ. The combustion efficiency in model A2SH is always higher than 96% and improves to nearly 100% for the maximum values of ϕ investigated. Altogether, such good performance may be attributed to a combination of higher values of R and also improved values of k with respect to model A2. The performance of this model in terms of NO_x emissions and combustion efficiency compares well with the best performances found in the literature for other approaches, namely those based on the lean-premixed concept (see, for example, [18–22]). Specifically, Bucher et al. [18] reported NO_x emissions below 10 ppm (15% O_2) and combustion efficiencies between 99.5 and 100% over a range of equivalence ratios for an optimized version of the lean-premixed trapped vortex combustor, and Hayashi et al. [22] reported NO_x emissions in general below 10 ppm (15% O_2) and combustion efficiencies between 95 and 100% over a wide range of equivalence ratios for a tubular lean–lean two-stage combustor model.

The results for models B1 and B2 are shown in Figs. 16 and 17, respectively. This configuration exhibits the same increase in CO and HC emissions with ϕ already reported for the previous cases, with the exception of model A2SH. However, very low values of NO_x emissions (lower than 7 ppm) are obtained throughout the investigated range of ϕ, probably as a consequence of poor combustion efficiency. Concerning model B1, this parameter reaches approximately 85% at low ϕ, decreasing to roughly 75% at the high end of the range. Significant improvements could not be obtained

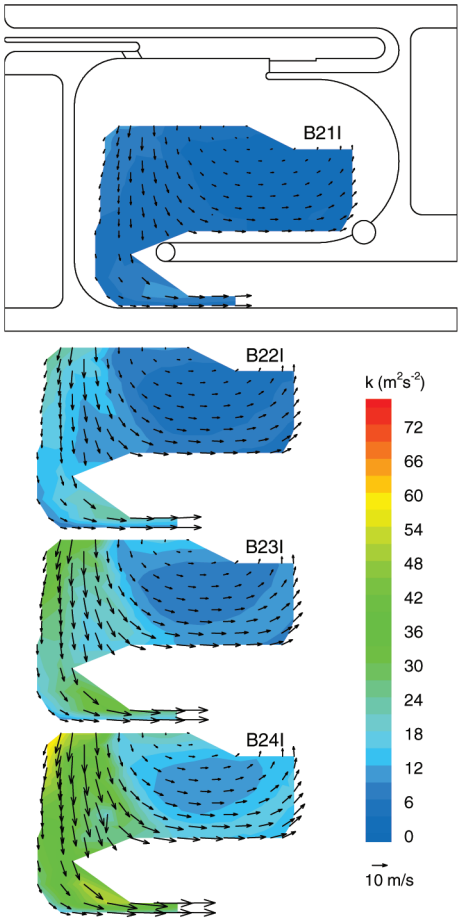

Fig. 11 Mean velocity vectors and turbulent kinetic energy fields at the symmetry plane inside the combustion chamber for model B2.

with the use of model B2. Despite the large values of R (see Table 3), the insufficient levels of k produced inappropriate combustion rates and, thus, the high emissions of CO and HC are not surprising.

IV. Conclusions

The performance of a novel combustor model for gas turbines with six different inlet air geometries has been assessed under nonreacting and reacting conditions. The mean and turbulent flow characteristics

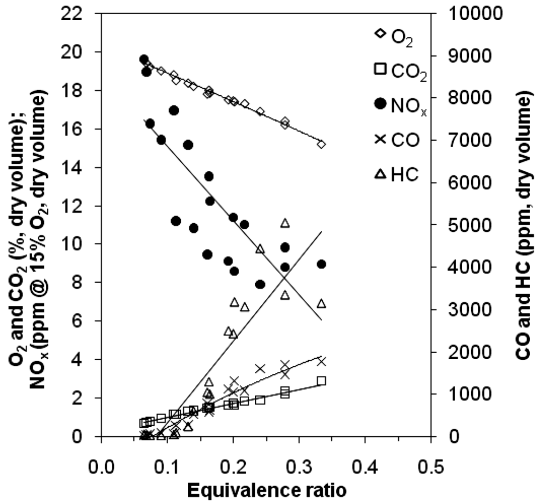

Fig. 13 Mean species concentration measurements at the exhaust of combustor model A1.

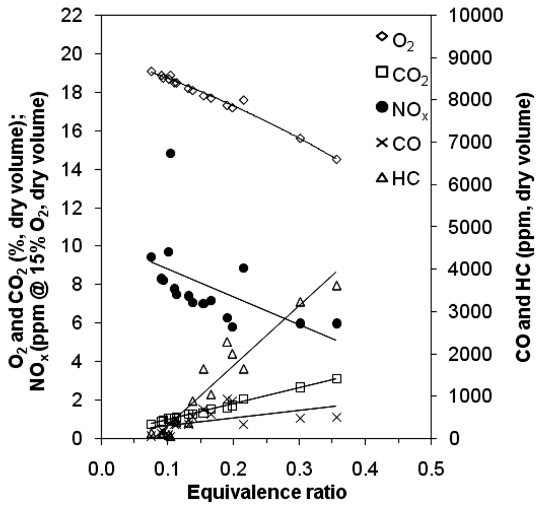

Fig. 14 Mean species concentration measurements at the exhaust of combustor model A2.

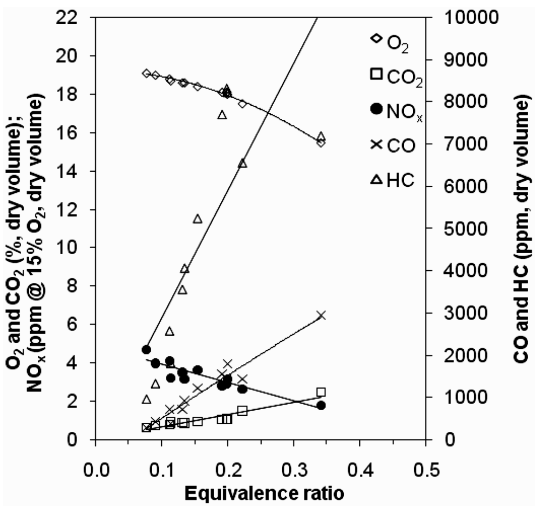

Fig. 12 Mean species concentration measurements at the exhaust of combustor model O.

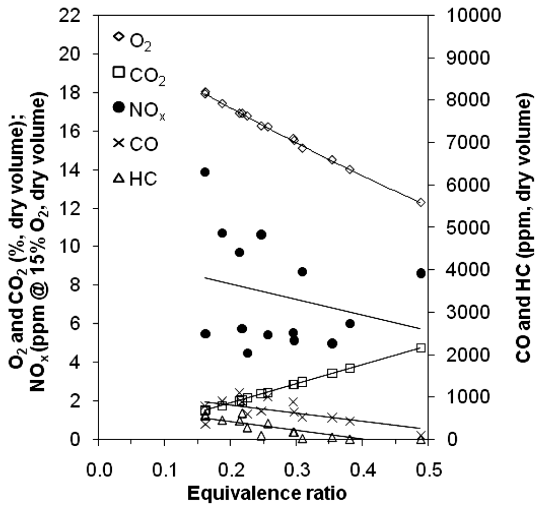

Fig. 15 Mean species concentration measurements at the exhaust of combustor model A2SH.

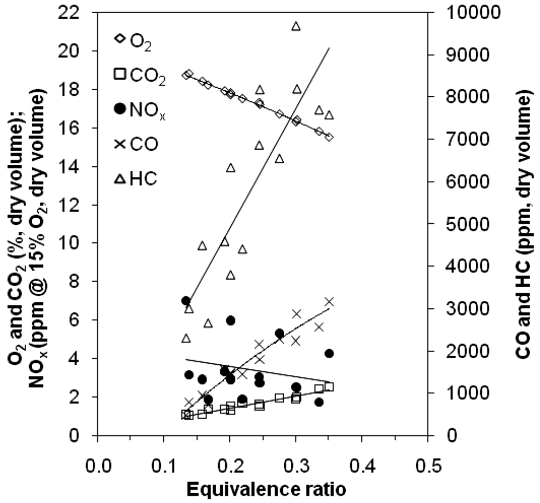

Fig. 16 Mean species concentration measurements at the exhaust of combustor model B1.

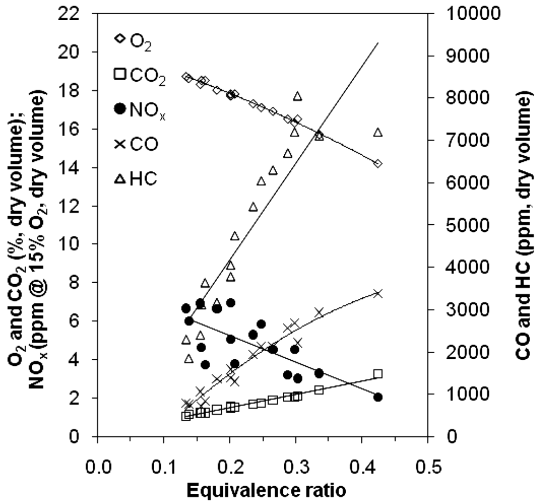

Fig. 17 Mean species concentration measurements at the exhaust of combustor model B2.

in the combustion chamber for nonreacting conditions have been investigated using laser-Doppler anemometry. This characterization was followed by measurements of (mean) gas species concentration (O_2, CO_2, CO, HC, and NO_x) at the exhaust of the combustor model. The isothermal data revealed that a common feature to all models and test conditions was the establishment of a large recirculation zone, as intended. It was also found that the recirculation ratio was primarily controlled by the inlet airflow geometry. The calculated values of this parameter ranged from about 0.4 (original configuration) to approximately 1.0 (configuration B). Characteristic values of turbulent kinetic energy inside the combustion chamber were also considered in the assessment of the various models, because of its impact in mixing rates between air, combustion products, and fuel. Model A2SH presented a combination of improved values of both recirculation ratio and turbulent kinetic energy.

The combustion experiments have demonstrated that the NO_x emissions were extremely low for all models, generally below 10 ppm. Unfortunately, this was attained at the expense of combustion efficiency, particularly in the original and B configurations. A significant improvement in combustion efficiency was obtained with configuration A, without incurring in the penalty of increasing the formation rates of NO_x. Model A2SH achieved ultralow NO_x emissions (less than 10 ppm) with combustion efficiencies higher than 99%, which is a remarkable accomplishment taking into consideration the simplicity of the geometry (no variable sections). In addition, the combustor did not show any signs of distortion or fractures after long periods of operation, even without cooling air.

Acknowledgments

Financial support for this work was provided by the European Commission under contract number ENK5-CT-2000-0014 and is acknowledged with gratitude. The first author (M. J. Melo) is pleased to acknowledge Fundação para a Ciência e a Tecnologia for the provision of a scholarship (SFRH/BD/6345/2001).

References

[1] Gupta, A. K., and Lilley, D. G., "Review: The Environmental Challenge of Gas Turbines," *Journal of the Institute of Energy*, Vol. 65, 1992, pp. 106–117.

[2] Gupta, A. K., and Lilley, D. G., "Combustion and Environmental Challenges for Gas Turbines in the 1990s," *Journal of Propulsion and Power*, Vol. 10, No. 2, 1994, pp. 137–147. doi:10.2514/3.23722

[3] Lefebvre, A. H., "The Role of Fuel Preparation in Low-Emission Combustion," *Journal of Engineering for Gas Turbines and Power*, Vol. 117, No. 4, 1995, pp. 617–655. doi:10.1115/1.2815449

[4] Beér, J. M., "Clean Combustion in Gas Turbines: Challenges and Technical Responses: a Review," *Journal of the Institute of Energy*, Vol. 67, 1995, pp. 2–10.

[5] Correa, S. M., "Power Generation and Aeropropulsion Gas Turbines: from Combustion Science to Combustion Technology," *Proceedings of the Combustion Institute*, Vol. 27, No. 2, 1998, pp. 1793–1807. doi:10.1016/S0082-0784(98)80021-0

[6] Hsu, K. Y., Gross, L. P., Trump, D. D., and Roquemore, W. M., "Performance of a Trapped Vortex Combustor," AIAA Paper 95-0810, 1995.

[7] Roquemore, W. M., Shouse, D., Burrus, D., Johnson, A., Cooper, C., Duncan, B., Hsu, K. Y., Katta, V. R., Sturgess, G. J., and Vihinen, I., "Trapped Vortex Combustor Concept for Gas Turbine Engines," AIAA Paper 2001-0483, 2001.

[8] Baltasar, J., Carvalho, M. G., Coelho, P., and Costa, M., "Flue-Gas Recirculation in a Gas-Fired Laboratory Furnace: Measurements and Modelling," *Fuel*, Vol. 76, No. 10, 1997, pp. 77–86, 919–929. doi:10.1016/S0016-2361(97)00093-8

[9] Levy, Y., Sherbaum, V., and Arfi, P., "Basic Thermodynamics of FLOXCOM, the Low-NO_x Gas Turbines Adiabatic Combustor," *Applied Thermal Engineering*, Vol. 24, Nos. 11–12, 2004, pp. 1593–1605. doi:10.1016/j.applthermaleng.2003.11.022

[10] Wünning, J. A., and Wünning, J. G., "Flameless Oxidation to Reduce Thermal NO-Formation," *Progress in Energy and Combustion Science*, Vol. 23, No. 1, 1997, pp. 81–94. doi:10.1016/S0360-1285(97)00006-3

[11] Katsuki, M., and Hasegawa, T., "The Science and Technology of Combustion in Highly Preheated Air," *Proceedings of the Combustion Institute*, Vol. 27, No. 2, 1998, pp. 3135–3146. doi:10.1016/S0082-0784(98)80176-8

[12] Cavaliere, A., and de Joannon, M., "Mild Combustion," *Progress in Energy and Combustion Science*, Vol. 30, No. 4, 2004, pp. 329–366. doi:10.1016/j.pecs.2004.02.003

[13] Galbiati, M. A., Cavigiolo, A., Effuggi, A., Gelosa, D., and Rota, R., "Mild Combustion for Fuel-NO_x Reduction," *Combustion Science and Technology*, Vol. 176, No. 7, 2004, pp. 1035–1054. doi:10.1080/00102200490426424

[14] de Joannon, M., Cavaliere, A., Faravelli, T., Ranzi, E., Sabia, P., and Tregrossi, A., "Analysis of Process Parameters for Steady Operations in Methane Mild Combustion Technology," *Proceedings of the Combustion Institute*, Vol. 30, No. 2, 2005, pp. 2605–2612. doi:10.1016/j.proci.2004.08.190

[15] Weber, R., Smart, J. P., and Kamp, W., "On the (MILD) Combustion of Gaseous, Liquid, and Solid Fuels in High Temperature Preheated Air," *Proceedings of the Combustion Institute*, Vol. 30, No. 2, 2005, pp. 2623–2629. doi:10.1016/j.proci.2004.08.101

[16] Costa, M., Melo, M. J., Sousa, J. M. M., and Levy, Y., "Spray Characteristics of Angled Liquid Injection into Subsonic Crossflows," *AIAA Journal*, Vol. 44, No. 3, 2006, pp. 646–653. doi:10.2514/1.10887

[17] Yanta, W. J., and Smith, R. A., "Measurements of Turbulent-Transport Properties with a Laser Doppler Velocimeter," AIAA Paper 73-169, 1973.

[18] Bucher, J., Edmonds, R. G., Steele, R. C., Kendrick, D. W., Chenevert, B. C., and Malte, P. C., "The Development of a Lean-Premixed Trapped Vortex Combustor," *Proceedings of ASME Turbo Expo, Power for Land, Sea, and Air*, American Society of Mechanical Engineers, Fairfield, NJ, July 2003.

[19] Leonard, G., and Stegmaier, J., "Development of an Aeroderivative Gas-Turbine Dry Low Emissions Combustion System," *Journal of Engineering for Gas Turbines and Power*, Vol. 116, No. 3, 1994, pp. 542–546. doi:10.1115/1.2906853

[20] Aida, N., Nishijima, T., Hayashi, S., Yamada, H., and Kawakami, T., "Combustion of Lean Prevaporized Fuel-Air Mixtures Mixed with Hot Burned Gas for Low-NO_x Emissions over an Extended Range of Fuel–Air Ratios," *Proceedings of the Combustion Institute*, Vol. 30, No. 2, 2005, pp. 2885–2892. doi:10.1016/j.proci.2004.08.040

[21] Johnson, M. R., Littlejohn, D., Nazeer, W. A., Smith, K. O., and Cheng, R. K., "A Comparison of the Flowfields and Emissions of High-Swirl Injectors and Low-Swirl Injectors for Lean Premixed Gas Turbines," *Proceedings of the Combustion Institute*, Vol. 30, No. 2, 2005, pp. 2867–2874. doi:10.1016/j.proci.2004.07.040

[22] Hayashi, S., Yamada, H., and Makida, M., "Extending Low-NO_x Operating Range of a Lean Premixed-Prevaporized Gas Turbine Combustor by Reaction of Secondary Mixtures Injected into Primary Stage Burned Gas," *Proceedings of the Combustion Institute*, Vol. 30, No. 2, 2005, pp. 2903–2911. doi:10.1016/j.proci.2004.08.112

T. Lieuwen
Associate Editor